On the Wave Propagation and Mode Conversion in a Helically Corrugated Multimode Circular Waveguide

C. C. H. TANG

Abstract—For specific forms of excitations, the normal modes and mode coefficients of a lossless helically corrugated circular multimode waveguide are determined from the appropriate boundary conditions. Because of the multiplicity of the roots of the characteristic dispersion equation obtained, care must be exercised in the evaluation of the equation and in the interpretation of the ω-β diagram.

For the TE_{11} mode excitation, it is shown that increasing either the depth or the width of the corrugation enhances the conversion into the TM_{11} mode, whereas increasing the pitch reduces the TM_{11} mode conversion. Mode conversion always increases with increasing frequency. The theoretical results are in agreement with the results of measurement.

Introduction

A DESCRIPTIVE model of a helically corrugated circular waveguide shown in Fig. 1 can be obtained by cutting a helical shallow slot along the inside wall of a standard rigid circular waveguide. The commercially available flexible circular waveguides have a similar inside surface of helical corrugation but can be used for negotiating a gentle bend. The purpose of this paper is 1) to analyze the characteristics of wave propagation in such a straight, helically corrugated, and multimode circular waveguide of infinite length and 2) to calculate the mode conversion level due to the presence of a section of helical corrugation in a smooth circular waveguide.

Related problems in magnetrons and linear accelerators for electrons [1]–[4], traveling-wave tubes [5], [6], and surface-wave structures [7]–[10] have been discussed in the literature with specific requirements for each problem. These three categories of problems mentioned above have been treated with one specific feature in common; i.e., they are all considered as slow-wave structures only. The basic feature of the present problem, which differs from that of the above-mentioned three classes of problems, is that both the fast-wave and slow-wave aspect of the wave propagation in a helically corrugated circular waveguide will be studied. The one characteristic that is common to all such structures is that the corrugated surfaces are capable of supporting a tangential component of electric field in the direction of energy propagation.

Usual approximate analyses for circularly corrugated linear accelerators assume the propagation of the lowest transverse magnetic slow-wave mode only, i.e., the circularly symmetric TM_{01} mode. Both the traveling-wave tubes and surface-wave guides are open-boundary structures, i.e., structures having one or more transverse field dimensions extending to infinity. The helically corrugated waveguide is a closed-boundary structure and because of its skew boundary conditions, it is necessary to analyze the problem by using both transverse magnetic modes and transverse electric modes in complete sets. For a specific form of excitation, the normal modes and mode coefficients of a lossless helically corrugated circular waveguide are determined from the appropriate boundary conditions. These boundary conditions lead to 1) a characteristic dispersion equation yielding the propagation constants of the normal modes and 2) equations yielding the mode coefficients that can be interpreted as the amount of conversion into various modes.

To investigate the transmission and mode conversion properties of a wave propagating through a transition from a smooth circular guide to a helically corrugated circular guide in a rigorous manner, we should expand the normal modes of the helically corrugated guide in terms of those of the smooth guide and vice versa. In such an expansion, an infinite set of linear equations in

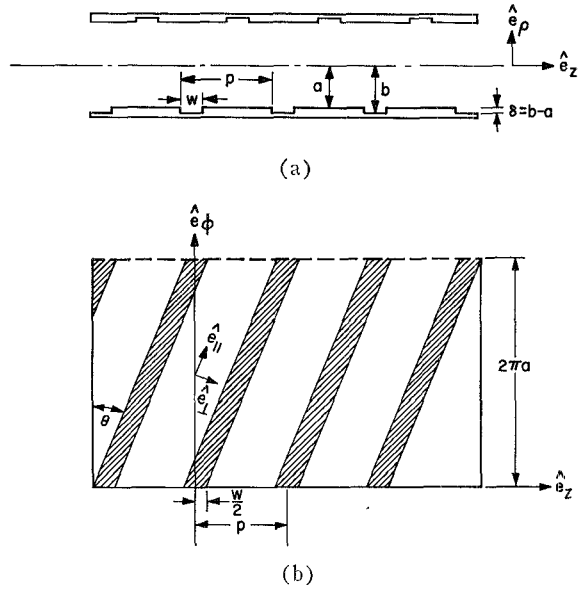

Fig. 1. (a) Cross-sectional view of a helically corrugated circular waveguide. (b) The developed view of the helical corrugation.

Manuscript received December 27, 1965; revised February 24, 1966.

The author is with Bell Telephone Laboratories, Inc., Murray Hill, N.J.

an infinite number of unknowns will be involved. Approximations are used to obtain the mode conversion in such cases.

Because of the nature of the characteristic dispersion equation obtained, care must be exercised in the evaluation of the equation and in the interpretation of the ω-β diagram. By varying the parameters such as the pitch p, slot depth δ, and slot width w, we conclude that the theoretical results and our physical intuition are compatible. The theoretical calculations and the experimental results obtained on available helically corrugated circular waveguides are also in agreement.

Because of the periodic nature of the helical corrugation, application of Floquet's theorem shows that the z-dependence of the fields must be of the form

$$e^{-j\beta_m z} = e^{-j\beta_0 z} e^{-j(m(2\pi/p))z}; \tag{3}$$

i.e.,

$$\beta_m = \beta_0 + m\frac{2\pi}{p}, \tag{4}$$

where m is any positive or negative integer.

The complete fields inside the radius a, with the time dependence $e^{j\omega t}$ suppressed, can be expressed as

$$\left.\begin{aligned}
E_z^i &= \sum_{m,n} E_{zmn}^i = \sum_{m,n} A_{mn}^i J_n(\zeta_m\rho) e^{-j(\beta_m z+n\phi)},\\
H_z^i &= \sum_{m,n} H_{zmn}^i = \sum_{m,n} B_{mn}^i J_n(\zeta_m\rho) e^{-j(\beta_m z+n\phi)},\\
E_\rho^i &= \sum_{m,n} E_{\rho mn}^i = \sum_{m,n}\left[-j\frac{\beta_m}{\zeta_m} A_{mn}^i J_n'(\zeta_m\rho) - \frac{n\omega\mu}{\zeta_m^2\rho} B_{mn}^i J_n(\zeta_m\rho)\right] e^{-j(\beta_m z+n\phi)},\\
E_\phi^i &= \sum_{m,n} E_{\phi mn}^i = \sum_{m,n}\left[-\frac{n\beta_m}{\zeta_m^2\rho} A_{mn}^i J_n(\zeta_m\rho) + j\frac{\omega\mu}{\zeta_m} B_{mn}^i J_n'(\zeta_m\rho)\right] e^{-j(\beta_m z+n\phi)},\\
H_\rho^i &= \sum_{m,n} H_{\rho mn}^i = \sum_{m,n}\left[+\frac{n\omega\epsilon}{\zeta_m^2\rho} A_{mn}^i J_n(\zeta_m\rho) - j\frac{\beta_m}{\zeta_m} B_{mn}^i J_n'(\zeta_m\rho)\right] e^{-j(\beta_m z+n\phi)},\\
H_\phi^i &= \sum_{m,n,} H_{\phi mn}^i = \sum_{m,n}\left[-j\frac{\omega\epsilon}{\zeta_m} A_{mn}^i J_n'(\zeta_m\rho) - \frac{n\beta_m}{\zeta_m^2\rho} B_{mn}^i J_n(\zeta_m\rho)\right] e^{-j(\beta_m z+n\phi)},
\end{aligned}\right\} \tag{5}$$

Formulation

The helically corrugated waveguide has a small pitch p, radius a, small pitch angle $\theta = \tan^{-1} p/2\pi a$, shallow slot depth $\delta = b - a$, and narrow slot width w as shown in Fig. 1(a), with its guide axis as the axis of the cylindrical coordinates (ρ, ϕ, z). The developed helical corrugation as viewed from inside when cut by a plane of constant ϕ and unrolled is shown in Fig. 1(b). An additional set of unit vectors $\hat{e}_\parallel$ and $\hat{e}_\perp$, parallel and perpendicular, respectively, to the pitch angle θ is introduced in Fig. 1(b) and the vector relation $\hat{e}_\perp = \hat{e}_p \times \hat{e}_\parallel$ holds. Let the superscripts i and s refer to the inside region $\rho \leq a$ and slot region $a \leq \rho \leq b$, respectively. We have the following boundary conditions:

at $\rho = a$,

$$\left.\begin{aligned}
E_z^i \tan\theta + E_\phi^i &= E_\parallel^s = 0,\\
E_z^i \cos\theta - E_\phi^i \sin\theta &= E_\perp,\\
H_z^i \sin\theta + H_\phi^i \cos\theta &= H_\parallel^s;
\end{aligned}\right\} \tag{1}$$

at $\rho = b$,

$$E_\parallel^s = E_\perp^s = 0. \tag{2}$$

with

$$\zeta_m^2 = k^2 - \beta_m^2, \tag{6}$$

and

$$k = \frac{\omega}{c} = \frac{2\pi}{\lambda_0}, \tag{7}$$

where ω and λ_0 are, respectively, the angular frequency and free-space wavelength. Equations (5) can be simplified [6] by noting the fact that if the helical corrugation is moved a distance less than p and then rotated in ϕ through a certain angle, it again coincides with itself. This constraint can be ensured only if we make $n = -m$ and put $A_{mn}^i = B_{mn}^i = 0$ for $n \neq -m$. Thus (5) is reduced to a single summation index in m.

In an attempt to make the present analysis applicable to frequencies far away from cutoffs of the multimode waveguide, an exact field distribution in terms of both propagating and evanescent modes across the opening of the helical slot is necessary. Such a field distribution is derived in the Appendix.

To express the field distribution across the slot opening in terms of space harmonic components, we write

$$E_{z(\rho=a)}^{s} = \sum_{m} \overline{E}_{zm}^{s}(a) e^{-j(\beta m z - m\phi)}. \tag{8}$$

Since

$$\cos\theta E_z^i(a) = E_\perp^s(a),$$
$$\cos\theta \overline{E}_{zm}^i(a) = \overline{E}_{\perp m}^s(a),$$

we have

$$\overline{E}_{\perp m}^s(a) = \frac{1}{p}\int_{-(w/2)+(p\phi/2\pi)}^{(w/2)+(p\phi/2\pi)} [E_\perp^s(a) e^{j(\beta_m z - m\phi)}]dz$$
$$= \frac{\pi}{2}\frac{w}{p} J_0\left(\beta_m \frac{w}{2}\right) E_\perp^s(a) e^{j\beta_0(p\phi/2\pi)}, \tag{9}$$

$$\frac{k}{j\omega\mu}\sum_{q=0}^{\infty} C_q^s \left\{ [H_q^{(2)}(kb)H_q^{(1)}(ka) - H_q^{(1)}(kb)H_q^{(2)\prime}(ka)] \times \left[1 - 2\sum_{n=1}^{\infty}\left(\frac{k}{k_n}\right)^2 J_0(n\pi)\right] - 2[H_q^{(2)}(kb)H_q^{(1)}(ka) - H_q^{(1)}(kb)H_q^{(2)}(ka)] \times \left[\sum_{n=1}^{\infty}\left(\frac{k}{k_n}\right)\frac{K_q(k_nb)I_q'(k_na) - I_q(k_nb)K_q'(k_na)}{K_q(k_nb)I_q(k_na) - I_q(k_nb)K_q(k_na)} J_0(n\pi)\right]\right\}$$
$$= \sum_m \left\{ -\frac{j\omega\epsilon}{\zeta_m}\cos\theta J_m'(\zeta_m a) A_m^i + \left[\sin\theta + \cos\theta\frac{m\beta_m}{a\zeta_m^2}\right] J_m(\zeta_m a) B_m^i \right\}. \tag{13}$$

Solutions of (11)–(13) furnish the sought-after characteristic dispersion equation:

$$\frac{\sum_{q=0}^{\infty} C_q^s \left\{ \left[H_q^{(2)}(kb)H_q^{(1)\prime}(ka) - H_q^{(1)}(kb)H_q^{(2)\prime}(ka)\right]\left[1 - 2\sum_{n=1}^{\infty}\left(\frac{k}{k_n}\right)^2 J_0(n\pi)\right] - 2[H_q^{(2)}(kb)H_q^{(1)}(ka) - H_q^{(1)}(kb)H_q^{(2)}(ka)]\left[\sum_{n=1}^{\infty}\left(\frac{k}{k_n}\right)\frac{K_q(k_nb)I_q'(k_na) - I_q(k_nb)K_q'(k_na)}{K_q(k_nb)I_q(k_na) - I_q(k_nb)K_q(k_na)} J_0(n\pi)\right]\right\}}{\sum_{q=0}^{\infty} C_q^s \left[H_q^{(2)}(kb)H_q^{(1)}(ka) - H_q^{(1)}(kb)H_q^{(2)}(ka)\right]\left[1 + 2\sum_{n=1}^{\infty} J_0(n\pi)\right]}$$
$$= \frac{\pi}{2}\frac{w}{p}\sum_m J_0\left(\beta_m\frac{w}{2}\right)\left\{\frac{(ka)^2[J_m'(\zeta_m a)]^2 - J_m^2(\zeta_m a)\left[(\zeta_m a)\tan\theta + m\frac{\beta_m}{\zeta_m}\right]^2}{(ka)(\zeta_m a)J_m(\zeta_m a)J_m'(\zeta_m a)\sec^2\theta}\right\} \tag{14}[1]$$

where $E_\perp^s(a)$ is obtained by putting $\rho = a$ and $z = 0$ in (24) in the Appendix, i.e., the field at the center of the opening of the slot. Accordingly, (9) becomes

$$\overline{E}_{\perp m}^s(a) = \frac{\pi}{2}\frac{w}{p} J_0\left(\beta_m\frac{w}{2}\right)\sum_{q=0}^{\infty} \times \left\{C_q^s[H_q^{(2)}(kb)H_q^{(1)}(ka) - H_q^{(1)}(kb)H_q^{(2)}(ka)] \times \left[1 + 2\sum_{n=1}^{\infty} J_0(n\pi)\right]\right\}. \tag{10}$$

The matching of the boundary conditions at $\rho = a$ at the center of the slot in accordance with (1) yields the following equations:

$$\left(\tan\theta + \frac{m\beta_m}{a\zeta_m^2}\right) J_m(\zeta_m a) A_m^i + j\frac{\omega\mu}{\zeta_m} J_m'(\zeta_m a) B_m^i = 0, \tag{11}$$

$$\overline{E}_{\perp m}^s(a) = \left[\cos\theta - \frac{m\beta_m}{a\zeta_m^2}\sin\theta\right] J_m(\zeta_m a) A_m^i - j\sin\theta\frac{\omega\mu}{\zeta_m} J_m'(\zeta_m a) B_m^i, \tag{12}$$

and the coefficients:

$$A_m^i = A_{mm}^i = \frac{\cos\theta}{J_m(\zeta_m a)}\overline{E}_{\perp m}^s(a), \tag{15}$$

$$B_m^i = B_{mm}^i = j\frac{[(\zeta_m a)^2\tan\theta + m(\beta_m a)]\cos\theta}{a\omega\mu(\zeta_m a)J_m'(\zeta_m a)}\overline{E}_{\perp m}^s(a). \tag{16}$$

The characteristic or determinantal equation (14) yields, for a given excitation field configuration, the propagation constant β_m for all possible normal modes in the helically corrugated waveguide, whereas (15) and (16) provide us with the relative contents of the normal modes for the particular excitation field configuration.

[1] The characteristic equation (14) turns out to be basically the same as equation (33) obtained by Foulds and Mansell in their paper "Propagation of an electromagnetic wave through a helical waveguide," *Proc. IEE (London)*, vol. 111, pp. 1789–1798, November 1964. When equation (14) was in the programming stage, the author noticed the publication of the paper by Foulds and Mansell using nonorthogonal helical coordinate system to obtain their equation (33) and emphasizing mainly on the propagation in the "deep" slot and the rotation of the plane of polarization of waves passing through the helical guide. The present paper uses a cylindrical coordinate system to obtain (14) above and has its emphasis on wave propagation and mode conversion characteristics in the helical guide and the proper interpretation of the ω-β diagram for the problem.

Inspection of (14) shows that it reduces to the normal mode solutions of a solid smooth circular waveguide as it should under the following conditions:

1) when $b = a$, then $J_m(\zeta_m a) = 0$ and $J_m'(\zeta_m a) = 0$
2) when $w = p$, then $J_m(\zeta_m b) = 0$ and $J_m'(\zeta_m b) = 0$
3) when $w = 0$, then $J_m(\zeta_m a) = 0$ and $J_m'(\zeta_m a) = 0$.

The actual computation of the propagation constant β_m will not be possible until the excitation field configuration is specified. To simplify the problem we assume in the next section that the only slot excitation field is in a form similar to the dominant mode TE_{11} in a solid smooth circular waveguide. Equation (14) then can be simplified by letting $q=1$ only.

Calculations, Discussions, and Measurements

For a given frequency, the phase velocities and amplitudes of the fundamental and space harmonics are not independent of each other, and depend on the form of potential field, which is controlled by the particular structure of the periodic guide and the particular excitation. The evaluation of the right side of (14) with $q=1$ only should center around the branch $m=1$ in this case, in order to insure the continuity of fields between the two regions, since we have chosen the TE_{11} mode slot excitation with circumferential variation corresponding to $q=1$. In other words, the fundamental is in the branch $m=1$ of the ω-β diagram as shown in Fig. 2, and the branch $m=q$ is always the fundamental branch. In fact, what is mentioned above is implicit in the meaning of the mode coefficients A_{mm} and B_{mm}. Physically, the implication is that the fundamental is taken to be that space harmonic with the highest phase velocity or the largest amplitude. Evaluation of the RHS series of (14) with $q=1$ only also confirms that for frequencies not too high the term with $m=1$ is always the fast-wave term with the highest phase velocity and the largest amplitude, whereas terms with $m \neq 1$ are all slow-wave space harmonic terms with relatively very small amplitude compared with that of $m=1$ term. The sum of all the slow-wave terms converges quite rapidly to zero. For slow waves, the argument of a Bessel function becomes imaginary and the relations are: $J_m(j\xi_m p) = J^m I_m(\xi_m p)$ and $J_m'(j\xi_m p) = -j \cdot j^m I_m'(\xi_m p)$. Inspection of Fig. 2 reveals that for the particular combination of a, δ, p, and w studied here, the ω-β curve of the helically corrugated circular guide virtually coincides with that of the corresponding mode of the solid circular guide; i.e., the propagation is virtually undisturbed by the presence of the shallow and narrow helical corrugation (the effect of deep corrugation will be discussed later) of appropriate pitch on the wall of a solid circular waveguide. $\Delta\beta = \beta - \beta_s$ in Fig. 2 shows that the difference between the phase constant of a smooth guide β_s and the phase constant of a corrugated guide β is very small and positive, indicating that the helically corrugated guide is less capacitive than the smooth guide. Measurements on such helically corrugated guides also confirm the above fact. It is logical to conjecture that the presence of the slow waves in the guide must have created such a field across the openings of the slots that the helically corrugated guide appears as a solid smooth guide to the fast wave—i.e., the field across the openings of the slots apparently appears vanishing.

To prove the validity of the statements in the preceding paragraph, we let a) $q=0$ only (for TM_{01}), and b) $q=2$ only (for TE_{11}) in (14) and we see from Figs. 3 and 4 that a) $m=0$, and b) $m=2$ are, respectively, the fundamental branch of the ω-β curves. These curves are again virtually identical with those of the corresponding modes of smooth circular waveguide since $\Delta\beta$'s are very small.

Apparently (14) with $q=1$ only can also be used for such a form of slot excitation as the TE_{1i} or TM_{1i} ($i=1, 2, 3, \cdots$) mode in a solid smooth circular waveguide for cases where multimode propagation are possible and accordingly solutions for β in these cases should be multivalued. This fact is verified by evaluation of β from (4), (6), and (14) [$q=1$ only] for multimode cases (i.e., at higher frequencies) as shown in the ω-β diagrams of Fig. 5(a) and (b).

The periodic nature of the ω-β diagram is obvious from Figs. 2–4. The phase velocities of the various harmonics are different in magnitudes and signs. At cutoff frequencies, for every space harmonic with positive phase velocity, there is one with an equal and opposite phase velocity. Equations (15) and (16) show that the amplitudes of these pairs are also equal and therefore, at cutoff frequency, the guide can support only standing waves. The group velocities of all the space harmonics are seen to be equal for any single frequency and to have the same direction as that of the energy. Those space harmonics whose phase velocities are always opposite in direction to the respective group velocities are termed reverse or backward waves. In particular, it is possible to have periodic structures in which the fundamental itself is a backward wave. Since the helically corrugated waveguide is a closed-boundary structure, its ω-β diagram does not have any "forbidden region" as evidenced in Figs. 2–4. Outside the triangles $v_p = \pm C$, the propagation is of slow-wave type, and the groove appears as inductive loading. Within the triangles the propagation is of fast-wave type and the groove appears as capacitive loading. The nature of slow-wave propagation becomes more and more evident as the depth or width of the corrugation increases as shown in Figs. 7 and 8 to be discussed later.

In Figs. 2–4, as the frequency increases, the value of (βp) will go through a multiple of π. The computation

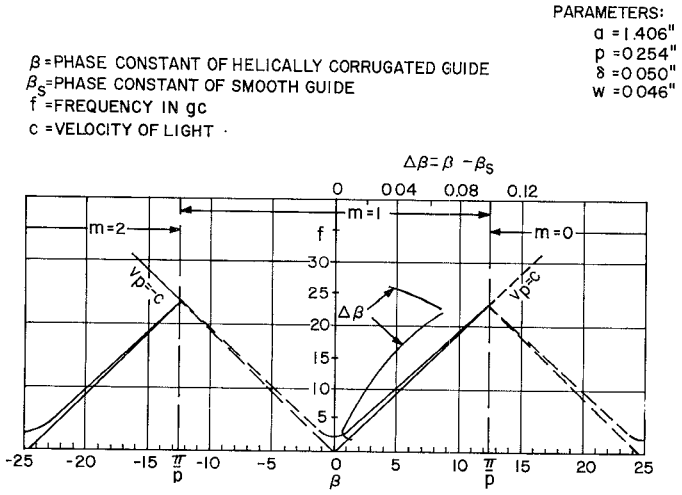

Fig. 2. Propagation characteristics of "TE_{11}" mode in a helically corrugated circular waveguide.

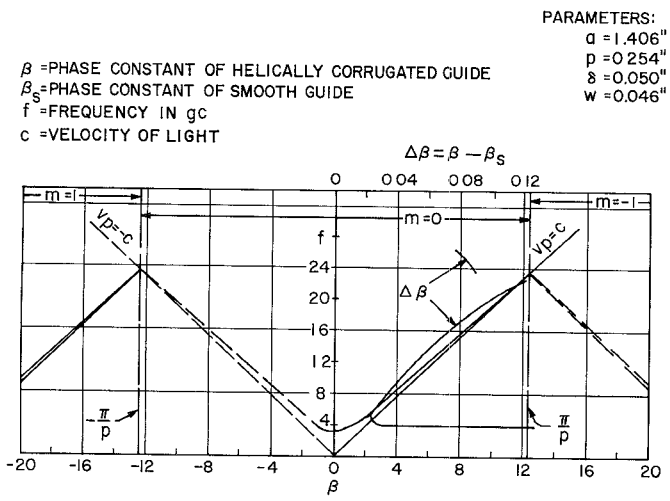

Fig. 3. Propagation characteristics of "TM_{01}" mode in a helically corrugated circular waveguide.

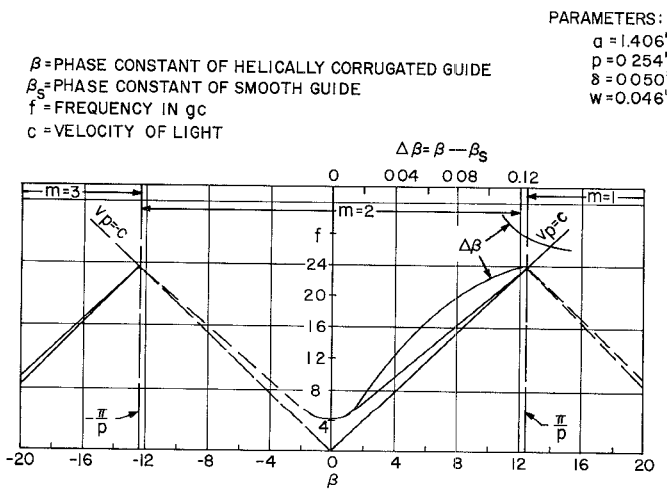

Fig. 4. Propagation characteristics of "TE_{21}" mode in a helically corrugated circular waveguide.

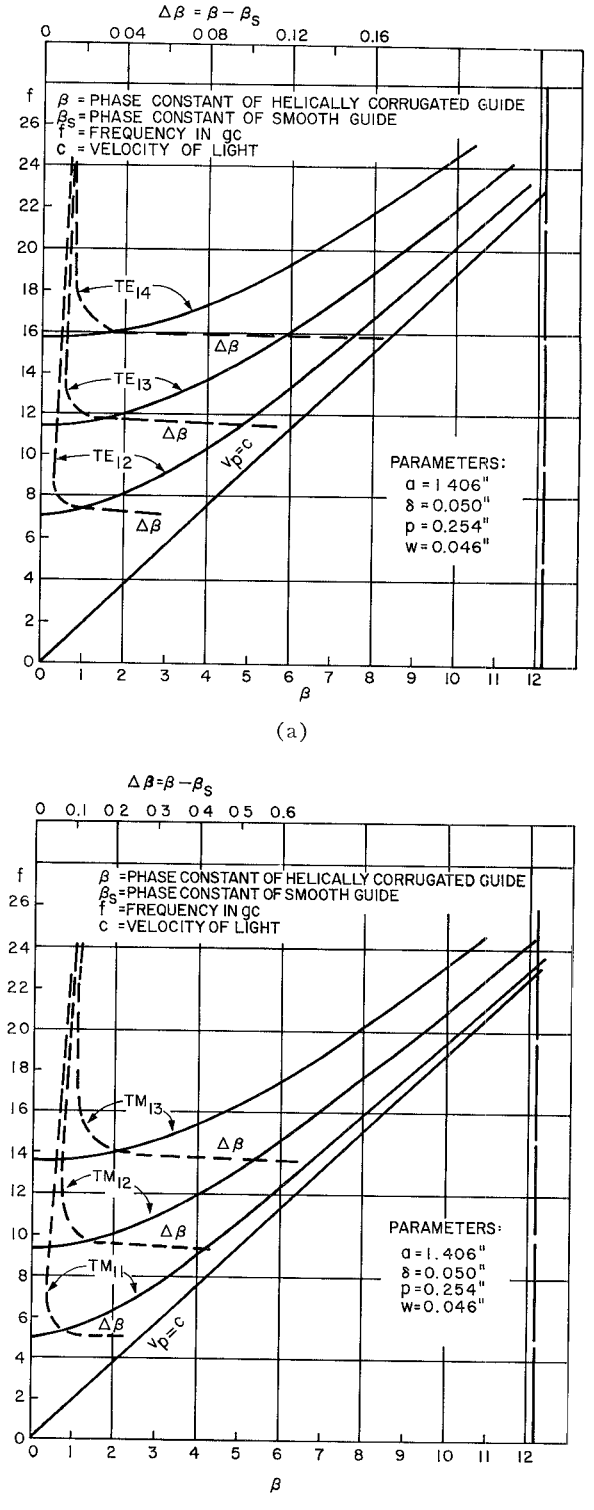

Fig. 5. (a) Propagation characteristics of "TE_{1l}" modes in a helically corrugated circular guide. (b) Propagation characteristics of "TM_{1l}" modes in a helically corrugated circular guide.

shows that when the frequencies at which (βp) approaches a multiple of π are reached, the fast-wave space harmonics begin to appear in addition to the fast-wave fundamental. At and around these frequencies the computation also shows that the amplitude of the fundamental drops and that of the space harmonic increases, typifying the description of a space harmonic "resonance" in the pitch length p. The typical sharp discontinutity in the propagation constant in the "conventional sense of resonance" does not occur here, as evidenced by the effect of varying the pitch p in Fig. 6 to be discussed later.

Before investigating mode conversions and observing the effect of varying parameters, w, p, and $\delta = b - a$, we shall briefly mention the way the propagation constants β_m of the normal modes of the helically corrugated circular waveguide are computed from (4), (6), and (14). The computation was carried out on IBM 7094 computer by assuming a reasonable $\beta_m = \beta_q$ on a cut-and-try basis in order to establish the identity of (14). Obviously, the propagation constant of the corresponding mode in solid smooth guide can serve as the best clue in choosing the initial trial value of $\beta_m = \beta_q$. Subsequent trials of β_m will be such that the values of the right-hand side of (14) converge to the constant value of the left-hand side for a particular frequency and particular mode of excitation. An "educated" guess of both the upper and lower limit of the sought-after β_m is often complicated by the multiplicity of the roots of (14). Accordingly, programming the equation to yield the sought-after propagation constant is, itself, a tremendous task.

The effect of varying the pitch of the helically corrugated guide with a narrow and shallow corrugation is shown in Fig. 6 and will be discussed first. We have mentioned earlier that for a fixed pitch p, the value of (βp) will go through a multiple of π as the frequency increases, as seen in Figs. 2–4. Figure 6 shows that as the pitch is increased, the fast-wave space harmonics will appear at lower frequencies as they should. Every time a fast-wave space harmonic is added, the βp is increased in its value by a π. The $\Delta\beta$ shown in Fig. 6 is for the fundamental "TE_{11}" (" " denotes the normal modes of the helically corrugated circular waveguide) fast wave only; i.e., $m = 1$, but the number label on each broken curve shows the fast-wave harmonics present. For example, the label with numbers 1, 0, and -1 indicates, respectively, that the fundamental, second harmonic, and third harmonic fast waves are present. At and around the frequencies for which (βp) goes through a multiple of π, the amplitude of the fundamental drops and that of the space harmonic rises, typifying the description of a space harmonic "resonance" in the pitch length p. It is important to note that at low frequencies, increasing the pitch p has the effect of reducing the $\Delta\beta$ (therefore reducing mode conversion also) without introducing the "resonance" effect of the second harmonic fast wave. Accordingly, for a particular frequency range of interest, there is always an "optimum" choice of the longest pitch length p in order to reduce the mode conversion [see Fig. 9(c)] level without "side effect."

The effect on the propagation constant by varying the slot width w of the helically corrugated guide with shallow slot depth and appropriate pitch is shown in Fig. 7. Increasing the slot width w increases the $\Delta\beta$ and therefore enhances the mode conversion [see Fig. 9(a)]. As the width is widened to a certain limit (e.g., $w = 0.10$ inch), the fundamental "TE_{11}" fast-wave will make the transition, at a certain frequency (at about 15.5 Gc/s for $w = 0.10$ inch), from the fast wave to the "TM_{11}" slow-wave fundamental and harmonics (in this case numbering from -3 to 5, i.e., forward and backward second through fifth space harmonics). The fact that the wave makes the transition from a fast one to a slow one indicates that the helically corrugated wall appears to change, for a certain fixed frequency, from capacitive to inductive for increasing slot width. When the width is equal to the pitch, all the slow waves vanish and the fast-wave fundamental alone propagates in the smooth guide of radius b. This is why in Fig. 7 the slow-wave portion of the curve for $\delta = 0.20$ inch is located above that for $\delta = 0.15$ inch or 0.10 inch.

Increasing the slot depth δ obviously will make the helically corrugated wall look, for a fixed frequency, less and less capacitive and eventually inductive for $\delta < \frac{1}{4}\lambda_0$. Figure 8 shows that for $\delta = 0.10$ inch, the wall becomes inductive at about 15.5 Gc/s and the fundamental "TE_{11}" fast wave makes the transition into the "TM_{11}" slow-wave fundamental and harmonics (in this case numbering from -2 to 4, i.e., forward and backward second through fourth harmonics). Increasing the slot depth also increases the $\Delta\beta$ and therefore enhances the mode conversion [see Fig. 9(b)]. If the depth of the corrugation goes through a multiple of quarter wavelength, the helically corrugated guide would behave like filters having stop bands and pass bands. For slot depth of 0.30 inch, for example, the slow-wave stop band starts around 9.5 Gc/s as seen in Fig. 8. In general, the propagation characteristics for guides with "deep" corrugation are drastically different from those with very shallow corrugation. For guides with "deep" corrugation, the waves will also propagate in the slot in the helical direction and the polarization plane of the waves propagating in the center space will be rotated, as discussed by Foulds and Mansell [13]. All these effects are the results of apparent significant increase of power flow into the helical corrugation.

We shall now turn our attention to the evaluation of the mode coefficients of (15) and (16). Assuming the dimensions shown in Fig. 2 and a slot excitation field with circumferential variation of the TE_{11} mode in smooth guide (i.e., $q = 1$), we can obtain numerical

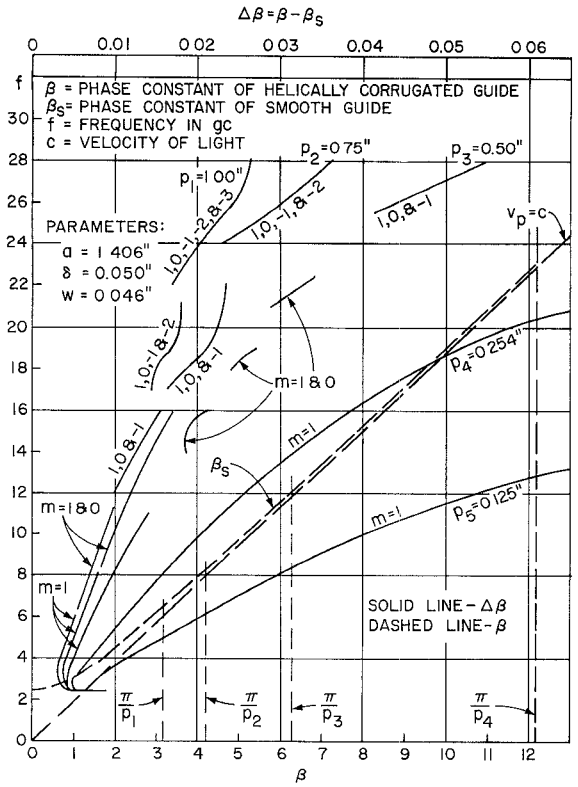

Fig. 6. Propagation characteristics for various pitch p.

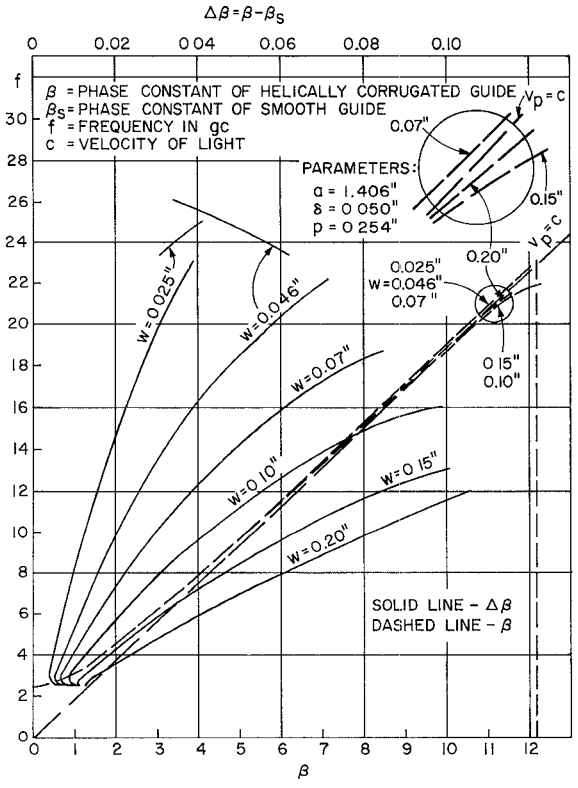

Fig. 7. Propagation characteristics for various slot width w.

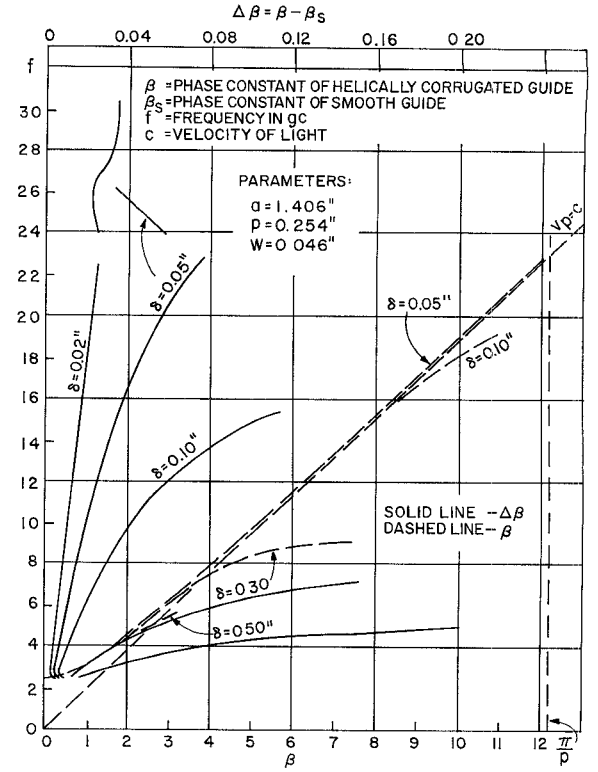

Fig. 8. Propagation characteristics for various slot depth δ.

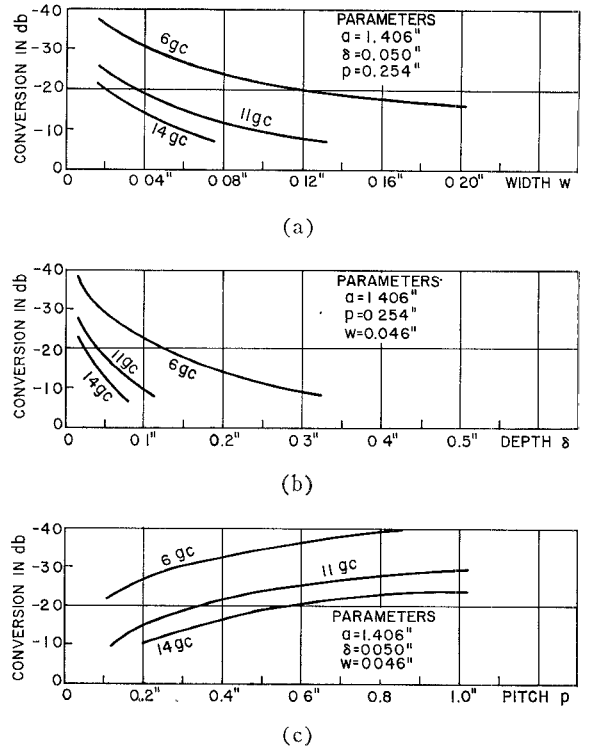

Fig. 9. (a) "TM_{11}" mode conversion in a helically corrugated circular guide. (b) "TM_{11}" mode conversion in a helically corrugated circular guide. (c) "TM_{11}" mode conversion in a helically corrugated circular guide.

values of the mode content from (15) and (16). We interpret the coefficient $B_{11}{}^{i}$ as the amount of "TE_{11}" (quotation marks denote the normal modes of the helically corrugated guide) mode fast-wave (or slow-wave) fundamental present in the helically corrugated guide and the coefficient $A_{11}{}^{i}$ as the amount of "TM_{11}" mode fast-wave (or slow-wave) fundamental. All other coefficients $A_{mm}{}^{i}$ and $B_{mm}{}^{i}$ for $|m|>1$ represent the amounts of fast-wave (or slow-wave) space harmonics. For the TE_{1i} or TM_{1i} mode excitation, $m=1$ means fundamental, $m=0$, -1, or -2 means, respectively, forward second, third, or fourth space harmonics, and $m=2$, 3, or 4 means, respectively, backward second, third, or fourth space harmonics. For TE_{2i} or TM_{2i} mode excitation, $m=2$ means fundamental and $m=1$, 0, or -1 means, respectively, forward second, third, or fourth space harmonics. For purposes of comparison, we are interested in only the relative magnitudes of the mode coefficients and, accordingly, all the mode coefficients will be normalized to the largest mode coefficient. The normalized mode coefficient thus represents the relative content of the mode with respect to the strongest mode. For the TE_{11} mode excitation and the parameters shown in Fig. 2, Table I shows that the "TM_{11}" mode is the only important one in addition to the dominant "TE_{11}" mode. All other coefficients $A_{mm}{}^{i}$ and $B_{mm}{}^{i}$ for $m\neq 1$ are all at least a few orders of magnitudes smaller than $A_{11}{}^{i}$.

For the TM_{11} mode excitation and parameters shown in Fig. 2, Table II shows that the "TE_{11}" mode is the only important one in addition to the "TM_{11}" mode.

Comparison of Tables I and II shows that "TM_{11}" is the "preferred" mode of the helically corrugated circular waveguide, because of its axial electric field component.

Both Tables I and II show that the mode "conversion" increases with increasing frequency. Figure 9 shows, for the TE_{11} mode excitation at 6, 11, and 14 Gc/s, the mode "conversion" by varying the parameters δ, p, and w, one at a time. It is seen that increasing either the width or the depth of the slot enhances the "TM_{11}" mode "conversion," whereas increasing the pitch rereduces the "TM_{11}" mode "conversion" as discussed earlier.

We are now in a position to study the transmission and mode conversion properties of waves at a transition from a smooth guide to a helically corrugated guide of semi-infinite length. To be rigorous, we have to express a typical normal mode of the smooth guide in terms of the normal modes of the helically corrugated guide. To do that exactly, we have to solve an infinite set of linear equations in an infinite number of unknowns. The problem can be simplified considerably if we may neglect the reflected waves at the transition for cases where the slot depth $\delta=b-a$ is small. In such cases, mode conversion should be small and the amount of mode conversion can be represented directly by (15) and (16) or Tables I and II and Fig. 9 as an approximation.

When a smooth waveguide, a length of helically corrugated waveguide, and a smooth waveguide are connected in tandem, the amount of converted mode at the output smooth guide is approximately the vector sum of the mode conversion voltages at the input transition (TE_{11} to "TM_{11}") and at the output transition ("TE_{11}" to TM_{11}). For example, we have from Tables I and II at 6 Gc/s the upper and lower bounds, respectively, at -28 dB and -31 dB level, depending upon the length of the corrugated circular waveguide section. We have obtained experimentally these two bounds by Klinger's cavity resonance method [14]. The test was performed by using a helically corrugated circular waveguide of four feet in length. The "educated" curve sketched from the measurement points shows that the upper bound is close to -28 dB level and the lower bound is about at -35 dB level (see Fig. 10). The agreement between the theoretical results and the experimental results is within the measurement accuracy of the method used.

TABLE I
MODE LEVELS FOR TE_{11} EXCITATION

f	6 Gc/s	11 Gc/s	14 Gc/s
"TE_{11}" Power: $(B_{11}{}^{i}/B_{11}{}^{i})^2$	0 dB	0 dB	0 dB
"TM_{11}" Power: $(A_{11}{}^{i}/B_{11}{}^{i})^2\,\epsilon/\mu$	-29 dB	-17 dB	-12 dB

TABLE II
MODE LEVELS FOR TM_{11} EXCITATION

f	6 Gc/s	11 Gc/s	14 Gc/s
"TM_{11}" Power: $(A_{11}{}^{i}/A_{11}{}^{i})^2$	0 dB	0 dB	0 dB
"TE_{11}" Power: $(B_{11}{}^{i}/A_{11}{}^{i})^2\,\mu/\epsilon$	-45 dB	-30 dB	-25 dB

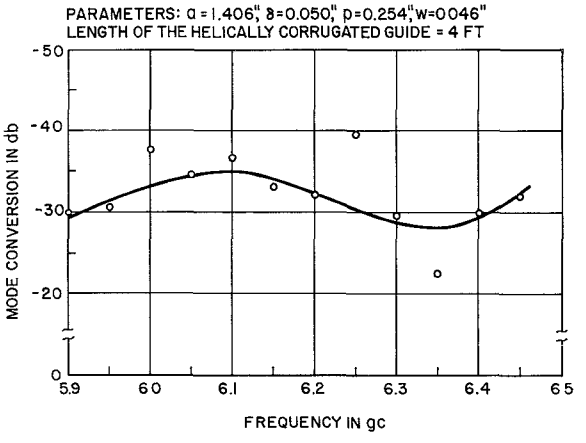

Fig. 10. "TM_{11}" mode conversion due to a section of helically corrugated circular waveguide.

CONCLUSION

For specific forms of excitations, the normal modes and mode coefficients of a lossless helically corrugated

circular waveguide are determined from the appropriate boundary conditions. Because of the multiplicity of the root of the characteristic dispersion equation obtained, care must be exercised in the evaluation of the transcendental equation and to the interpretation of the ω-β diagram.

By varying the parameters such as the pitch p, slot depth δ, and slot width w, we find that our physical intuition and the theoretical results are compatible. Measurements on a section of helically corrugated circular waveguide also show that the experimental data and the theoretical results are in agreement. For the TE_{11} mode excitation, it is shown that increasing either the width or the depth of the corrugation enhances the TM_{11} mode conversion, whereas increasing the pitch reduces the TM_{11} mode conversion. Mode conversion always increases with increasing frequency.

Appendix

Field Distribution at a Helical Slot Opening

For field excitations with arbitrary circumferential variations at the opening of a slot, the electric field inside the helical slot of width $w<\frac{1}{2}\lambda_0$ in general has the following form of E-type modes (similar to those in radial transmission lines) in a localwise sense:

$$E_{\perp}^{s} = \sum_{q=0}^{\infty} C_q^{s}[H_q^{(2)}(kb)H_q^{(1)}(k\rho) - H_q^{(1)}(kb)H_q^{(2)}(k\rho)]e^{-j(\beta_q z - q\phi)}, \quad \text{for } \frac{p\phi}{2\pi} - \frac{w}{2} < z < \frac{p\phi}{2\pi} + \frac{w}{2},$$
$$= 0 \quad \text{for } \frac{p\phi}{2\pi} + \frac{w}{2} < z < p + \frac{p\phi}{2\pi} - \frac{w}{2}. \tag{17}$$

Since $E_{\perp}^{s}$ must be constant in magnitude and phase inside the slot of width $w\cos\theta(<\frac{1}{2}\lambda_0)$, we use the phase at the center of the slot, i.e., letting $z=\varphi/2\pi$ in (17). The field across the opening of the slot is apparently constant according to (17), by putting $\rho=a$. On the other hand, because of the fringing at the corners of the slot, the actual field $E_{\perp}^{s}$ across the opening becomes infinitely large at the corners in a quasi-static manner as [11]

$$E_{\perp(\rho=a)}^{s} = \frac{G}{\left[1-\left(\frac{2z}{w}\right)^2\right]^{1/2}}; \tag{18}$$

i.e., it approaches infinity according to $D^{-1/2}$, where D is the distance from the corner, in a fashion similar to infinitely sharp edges in diffraction problems [12]. Obviously, the field near the opening of the slot cannot be represented completely by (17) by merely letting $\rho=a$, since there are many evanescent higher order E-type modes with z-variations present at the opening of the slot in order to satisfy the boundary conditions at $\rho=a$ shown in (18). To find the evanescent modes, we expand (18) into a Fourier series:

$$E_{\perp(\rho=a)}^{s} = \sum_{n=0}^{\infty} a_n \cos k_z z, \tag{19}$$

where

$$k_z = n\frac{2\pi}{w}, \tag{20}$$

$$a_0 = G\frac{\pi}{2}, \quad \text{for the propagating modes.} \tag{21}$$

$$a_{n\neq 0} = G\pi J_0(n\pi), \quad \text{for the evanescent modes.} \tag{22}$$

Here, we assume for simplicity that the propagation of $E_{\perp}^{s}$ is in the z-direction for small pitch angle θ. Equating (17) to (21) we get, at $\rho=a$ and $z=\phi/2\pi$,

$$G = e^{-j\beta_0(p\phi/2\pi)}\frac{2}{\pi}\sum_{q=0}^{\infty} C_q^{s}[H_q^{(2)}(kb)H_q^{(1)}(ka) - H_q^{(1)}(kb)H_q^{(2)}(ka)]. \tag{23}$$

The complete electric field expansion in the slot therefore is

$$E_{\perp}^{s} = \sum_{n=0}^{\infty} E_{\perp n}^{s} = e^{-j\beta_0(p\phi/2\pi)}\sum_{q=0}^{\infty}$$
$$\times \left\{C_q^{s}[H_q^{(2)}(kb)H_q^{(1)}(k\rho) - H_q^{(1)}(kb)H_q^{(2)}(k\rho)]\right.$$
$$\times\left[1 + 2\sum_{n=1}^{\infty}\frac{K_q(k_n b)I_q(K_n\rho) - I_q(k_n b)K_q(k_n\rho)}{K_q(k_n b)I_q(k_n a) - I_q(k_n b)K_q(k_n a)}\right.$$
$$\left.\left.\times J_0(n\pi)\cos\left(n2\pi\frac{z}{w}\right)\right]\right\},$$
$$\text{for } \frac{p\phi}{2\pi} - \frac{\omega}{2} < z < \frac{p\phi}{2\pi} + \frac{\omega}{2}$$
$$\text{for } \frac{p\phi}{2\pi} + \frac{\omega}{2} < z < p + \frac{p\phi}{2\pi} - \frac{\omega}{2} \tag{24}$$
$$= 0$$

where

$$k_n^2 = k_z^2 - k^2 = \left(n\frac{2\pi}{w}\right)^2 - k^2, \qquad n\neq 0 \tag{25}$$

and

$$K_q(k_n\rho) = \frac{\pi}{2}j^{q+1}H_q^{(1)}(jk_n\rho). \tag{26}$$

The magnetic field in the slot is

$$H_{\parallel}{}^{s} = \sum_{n=0}^{\infty} H_{\parallel n}{}^{s} = \sum_{n=0}^{\infty} -\frac{j\omega\epsilon}{k_n{}^2}\frac{\partial E_{\perp n}{}^{s}}{\partial\rho} = \frac{1}{j\omega\mu}\left[\frac{\partial E_{\perp o}{}^{s}}{\partial\rho} + \sum_{n=1}^{\infty} -\left(\frac{k}{k_n}\right)^2\frac{\partial E_{\perp n}{}^{s}}{\partial\rho}\right]$$

$$= e^{-j\beta_0(p\phi/2\pi)}\frac{1}{j\omega\mu}\sum_{q=0}^{\infty} C_q{}^{s}\Big\{k\left[H_q{}^{(2)}(kb)H_q{}^{(1)\prime}(k\rho) - H_q{}^{(1)}(kb)H_q{}^{(2)\prime}(k\rho)\right]$$

$$\times\left[1 + 2\sum_{n=1}^{\infty} -\left(\frac{k}{k_n}\right)^2\frac{K_q(k_nb)I_q(k_n\rho) - I_q(k_nb)K_q(k_n\rho)}{K_q(k_nb)I_q(k_na) - I_q(k_nb)K_q(k_na)}J_0(n\pi)\cos\left(n2\pi\frac{z}{w}\right)\right]$$

$$+ \left[H_q{}^{(2)}(kb)H_q{}^{(1)}(k\rho) - H_q{}^{(1)}(kb)H_q{}^{(2)}(k\rho)\right]$$

$$\times\left[2\sum_{n=1}^{\infty} -\left(\frac{k}{k_n}\right)^2 k_n\frac{K_q(k_nb)I_q{}'(k_n\rho) - I_q(k_nb)K_q{}'(k_n\rho)}{K_q(k_nb)I_q(k_na) - I_q(k_nb)K_q(k_na)}J_0(n\pi)\cos\left(n2\pi\frac{z}{w}\right)\right]\Big\}. \quad (27)$$

Acknowledgment

The author gratefully acknowledges the competent assistance he received from Mrs. B. Hofmann, who spent about one-third of her time over a period of a year in programming the problem. The author also wants to thank L. Dale for the measurements.

References

[1] J. C. Slater, "Theory of the magnetron oscillator," Mass. Inst. Tech., Cambridge, M.I.T. Radiation Lab. Rept. V 5S, pp. 1–32, August 1941.
[2] H. Goldstein, "Cavity resonators and waveguides containing periodic elements," Ph.D. dissertation, Mass. Inst. Tech., Cambridge, 1943.
[3] W. Walkinshaw, "Theory of circular corrugated waveguides for linear accelerators," British TRE Rept. T2037, August 1946.
[4] E. L. Chu and W. W. Hansen, "The theory of disk-loaded waveguides," *J. Appl. Phys.*, vol. 18, pp. 996–1008, November 1947.
[5] J. R. Pierce, *Traveling-Wave Tubes*. Princeton, N. J.: Van Nostrand, 1950.
[6] S. Sensiper, "Electromagnetic wave propagation on helical conductors," Sc.D. dissertation, Mass. Inst. Tech., Cambridge, 1951.
[7] C. C. Cutler, "Electromagnetic waves guided by corrugated conducting surfaces," Bell Telephone Labs., MM-44-160-218, October 1944.
[8] L. Brillouin, "Waveguides for slow waves," *J. Appl. Phys.*, vol. 19, pp. 1023–1041, November 1948.
[9] G. Goubau, "Surface waves and their application to transmission lines," *J. Appl. Phys.*, vol. 21, pp. 1119–1128, November 1950.
[10] A. F. Harvey, "Periodic and guiding structures at microwave frequencies," *IRE Trans. on Microwave Theory and Techniques*, vol. MTT-8, pp. 30–61, January 1960.
[11] W. R. Smythe, "Narrow gaps in microwave problems," *Rev. Modern Phys.*, vol. 20, pp. 175–180, January 1948.
[12] C. J. Bouwkamp, "Diffraction theory," *Repts. Progr. Phys.*, vol. 17, p. 45, 1954.
[13] K. Foulds and J. Mansell, "Propagation of an electromagnetic wave through a helical waveguide," *Proc. IEE* (London), vol. 111, pp. 1788–1798.
[14] Y. Klinger, "The measurement of spurious modes in overmoded waveguides," *Proc. IEE (London)*, vol. 106, pt. B supplement, pp. 89–99, January 1959.